Phase noise suppression of optical OFDM signals in 60-GHz RoF transmission system

Chun-Ting Lin,[1,*] Chia-Chien Wei,[2] and Ming-I Chao[1]

[1]*Institute of Photonic System, National Chiao Tung University, Tainan, Taiwan*
[2]*Department of Applied Materials and Optoelectronic Engineering, National Chi Nan University, Nautou, Taiwan*
** jinting@mail.nctu.edu.tw*

Abstract: The dispersion-induced phase noise (PN) in an OFDM RoF system at 60 GHz leads to not only subcarrier phase rotation (PRT) but also intercarrier interference (ICI) to severely degrade the transmission performance, when a commercial cost-effective DFB laser with the linewidth of several MHz is adopted. To mitigate both PRT and ICI, a post PN suppression algorithm is proposed, and it does not require any bandwidth-consuming pilot tone. For a 25.78-Gbps 16-QAM OFDM RoF signal using the laser with 1.8-MHz linewidth, employing the algorithm can extend the maximum transmission distance which corresponds to 3-dBm power penalty at the BER of 2×10^{-3} from 75 km to more than 115 km, i.e. 50% increment of transmission distance.

OCIS codes: (060.2330) Fiber optics communications; (060.3510) Lasers, fiber; (060.5625) Radio frequency photonics.

References and links

1. M. Sauer, A. Kobyakov, and J. George, "Radio over fiber for picocellular network architectures," J. Lightwave Technol. **25**(11), 3301–3320 (2007).
2. Y. X. Gu, B. Luo, C. S. Park, L. C. Ong, M.-T. Zhou, and S. Kato, "60 GHz Radio-over-Fiber for Gbps Transmission," in Proceedings of Global Symp. Millimeter Waves (GSMM), pp. 41–43,(2008).
3. C. T. Lin, J. Chen, P.-T. Shih, W. J. Jiang, and S. Chi, "Ultra-hgh data-rate 60 GHz radio-over-fiber systems employing optical frequency multiplication and OFDM formats," J. Lightwave Technol. **28**(16), 2296–2306 (2010).
4. Z. Jia, J. Yu, Y. T. Hsueh, A. Chowdhury, H. C. Chien, J. A. Buck, and G. K. Chang, "Multiband signal generation and dispersion-tolerant transmission based on photonic frequency tripling technology for 60-GHz radio-over-fiber systems," IEEE Photon. Technol. Lett. **20**(17), 1470–1472 (2008).
5. H. C. Chien, A. Chowdhury, Z. Jia, Y. T. Hsueh, and G. K. Chang, "Long-Reach, 60-GHz Mm-Wave Optical-Wireless Access Network Using," European Conference on Optical Communication (ECOC'08), paper Tu.3.F.3, 2008.
6. W. R. Peng, J. Chen, and S. Chi, "On the phase noise impact in direct-detection optical OFDM transmission," IEEE Photon. Technol. Lett. **22**(9), 649–651 (2010).
7. D. Qian, N. Cvijetic, J. Hu, and T. Wang, "Optical OFDM Transmission in Metro/Access Networks," Optical Fiber Communication (OFC'09), paper OMV1, 2009.
8. C. C. Wei, and J. J. Chen, "Study on dispersion-induced phase noise in an optical OFDM radio-over-fiber system at 60-GHz band," Opt. Express **18**(20), 20774–20785 (2010).
9. R. Lin, "Next Generation PON in Emerging Networks," Optical Fiber Communication (OFC'09), paper OWH1, 2008.
10. S. Wu, P. Liu, and Y. Bar-Ness, "Phase noise estimation and mitigation for OFDM systems," IEEE Trans. Wirel. Comm. **5**(12), 3616–3625 (2006).
11. W.-R. Peng, I. Morita, and H. Tanaka, "Digital Phase Noise Estimation and Mitigation Approach for Direct-Detection Optical OFDM Transmissions," European Conference on Optical Communication (ECOC'10), paper Tu.3.C.3, 2010.
12. W. J. Jiang, C. T. Lin, L. Y. Wang He, C. C. Wei, C. H. Ho, Y. M. Yang, P. T. Shih, J. Chen, and S. Chi, "32.65-Gbps OFDM RoF Signal Generation at 60GHz Employing an Adaptive I/Q Imbalance Correction," European Conference on Optical Communication (ECOC'10), paper Th.9.B.5, 2010.
13. C.-T. Lin, P.-T. Shih, J. Chen, W.-Q. Xue, P.-C. Peng, and S. Chi, "Optical millimeter-wave signal generation using frequency quadrupling technique and no optical filtering," IEEE Photon. Technol. Lett. **20**(12), 1027–1029 (2008).

#145131 - $15.00 USD Received 1 Apr 2011; revised 9 May 2011; accepted 9 May 2011; published 11 May 2011

1. Introduction

Wireless communication at 60-GHz band has attracted much attention due to up to 7-GHz unlicensed spectrum for popular bandwidth-hungry applications, such as High-Definition (HD) video [1]. Nevertheless, the significantly high air-link loss at 60 GHz (8~8.5 dB/m in modern office building) will severely limit the wireless transmission distance to less than ~10 m [2]. Accordingly, capacious feeders are required to facilitate wireless access. Recently, the radio-over-fiber (RoF) system has been considered as a promising candidate to provide the required feeder network due to low loss and almost unlimited bandwidth of optical fiber [3,4]. However, one of the major challenges of 60 GHz RoF system is the limitation of fiber transmission distance. The range of 60 GHz RoF system is limited to tens of kilometers, which is mainly owing to fading and time-shifting effects induced by fiber chromatic dispersion [5]. Such short reach of 60 GHz RoF access system will give rise to higher cost of network deployment. To extent the coverage, several 60 GHz RoF architectures have been proposed to overcome fading and time-shifting effects, which simultaneously transmit an RF-tone and optical data-modulated signal with 60-GHz frequency difference over fiber [3]. The beating term between them after a photo-detector is the desired electrical radio signals at 60-GHz band. To eliminate the phase noise (PN) caused by laser linewidth, both the RF-tone and the optical data-modulated signal are generated by modulating the same laser, and theoretically, laser PN will not affect the received 60 GHz signals [6]. However, the phase coherence between them is reduced after dispersive fiber transmission. Therefore, the dispersion-induced PN on electrical 60-GHz signals is generated after photo-detection

Recently, orthogonal frequency-division multiplexing (OFDM) has been considered as a prominent format for a variety of digital communication systems owing to its robustness against frequency selective fading and inter-symbol interference caused by both multipath in air-link and chromatic dispersion in optical fibers [7]. Besides, highly spectral efficiency and flexibility of OFDM makes it attractive for narrowband applications (i.e. 7-GHz license-free band at 60 GHz) beyond the 10-Gb/s regime. However, an OFDM signal is very sensitive to PN which will destroy the orthogonality among subcarriers. Hence, the dispersion-induced PN from nonzero laser linewidth causes not only phase rotation (PRT) on each subcarrier but also intercarrier interference (ICI) among subcarriers [6,8] to greatly reduce the fiber transmission distance. In particular, due to the increasing interest in optically amplified long-reach passive optical networks (PONs) [9], the required reach of a hybrid RoF/PON system which is expected to provide various services is up to 100 km.

In this work, by simplifying the profile of dispersion, we use the algorithm from the area of wireless communication [10] to estimate and suppress both PRT and ICI. Compared with the work proposed in [11], the proposed PN suppression (PNS) algorithm does not require any bandwidth-consuming pilot tones to allow full utilization of 7-GHz unlicensed band at 60 GHz. Experimental results show that the algorithm can suppress the performance degradation caused by dispersion-induced PN to extend the transmission distance and/or to reduce the requirement of laser linewidth. Employing the algorithm, the 25.78-Gbps 16-QAM OFDM signals at 60 GHz can reach the BER of 2×10^{-3} after 100-km transmission, and the extension of transmission distance is more than 40 km using the laser with 1.3 or 1.8-MHz linewidth.

2. PN suppression algorithm

While the coherent RF tone and the OFDM signal with 60-GHz frequency difference are sent into fiber simultaneously, fiber dispersion can de-correlate the RF tone and the OFDM subcarriers via different group velocities. Hence, their walk-off in the time domain will result in differential PN. The differential PN between the RF tone and the q-th subcarrier of the m-th OFDM symbol can be simply approximated as $\varphi_{m,q}(t) = \theta(t + t_q) - \theta(t)$, where $\theta(t)$ is the laser PN and t_q is the relative time delay between the RF tone and the q-th subcarrier. After

#145131 - $15.00 USD Received 1 Apr 2011; revised 9 May 2011; accepted 9 May 2011; published 11 May 2011

down-conversion, removing the cyclic prefix (CP) and taking discrete Fourier transform (DFT), the received q-th subcarrier of the m-th symbol after transmission is given as [6,8],

$$R_{m,q} = H_q S_{m,q} I_{m,q}(0) + \sum_{n=0,\, n\neq q}^{N-1} H_n S_{m,n} I_{m,n}(q-n) + W_{m,q}\,, \tag{1}$$

where N is the subcarrier number, and $S_{m,q}$, H_q and $W_{m,q}$ are the transmitted data, the channel response, and the white noise at the q-th subcarrier, respectively. $I_{m,q}$ is the DFT of $\exp(j\varphi_{m,q}(n))$, where $\varphi_{m,q}(n)$ denotes the n-th sample of $\varphi_{m,q}(t)$. While $I_{m,q}(0)$ provides PRT on each subcarrier, $I_{m,q}(k)|_{k\neq 0}$ results in ICI. Moreover, Eq. (1) can be rewritten as a compact matrix form,

$$\mathbf{R}_m = \tilde{\mathbf{I}}_m \tilde{\mathbf{H}} \mathbf{S}_m + \mathbf{W}_m\,, \tag{2}$$

where symbols in bold with and without tide represent matrices and vectors, respectively; $\tilde{\mathbf{I}}_m = [\mathbf{I}_{m,0}, \mathbf{I}_{m,1}, \cdots, \mathbf{I}_{m,N-1}]$ and $\mathbf{I}_{m,q} = [I_{m,q}(-q), I_{m,q}(1-q), \cdots, I_{m,q}(N-1-q)]^T$ denote the effect of PN; $\tilde{\mathbf{H}} = \mathrm{diag}\{[H_0, H_1, \cdots, H_{N-1}]\}$ denotes a diagonal matrix with H_q as the diagonal, and $\mathbf{R}_m = [R_{m,0}, R_{m,1}, \cdots, R_{m,N-1}]^T$, $\mathbf{S}_m = [S_{m,0}, S_{m,1}, \cdots, S_{m,N-1}]^T$ and $\mathbf{W}_m = [W_{m,0}, W_{m,1}, \cdots, W_{m,N-1}]^T$ are the vector forms of the received signal, the transmitted signal and the noise, respectively. Compared with the PN caused by uncorrelated local oscillator in wireless communications [10], the influence of dispersion-induced PN described by Eq. (1) on the received OFDM data has a major difference: $I_{m,q}(k)$ dependents on the frequency of the subcarrier, and this is the reason the PRT is not "common" phase error. However, since the frequency difference among subcarriers is much smaller than that between the RF tone and a subcarrier [1], the correlation between $I_{m,q}(k)$ and $I_{m,q'}(k)$ is high. We could assume $I_{m,q}(k) = J_m(k)$ implying complete coherence among subcarriers to simplify Eq. (2) as,

$$\mathbf{R}_m \cong \tilde{\mathbf{J}}_m \mathbf{D}_m + \mathbf{W}_m = \tilde{\mathbf{D}}_m \mathbf{J}_m + \mathbf{W}_m, \tag{3}$$

where $\mathbf{J}_m = [J_m(0), J_m(1), \cdots, J_m(N-1)]^T$ is independent on subcarriers, $\mathbf{D}_m = \tilde{\mathbf{H}}\mathbf{S}_m$ represents detected signals without noise. Since $\tilde{\mathbf{J}}_m \mathbf{D}_m$ and $\tilde{\mathbf{D}}_m \mathbf{J}_m$ represents the circular discrete convolution of $\mathbf{D}_m$ and $\mathbf{J}_m$, $\tilde{\mathbf{J}}_m$ and $\tilde{\mathbf{D}}_m$ are $N \times N$ matrices and their entries must satisfy $\tilde{\mathbf{J}}_m(x,y) = \mathbf{J}_m(\langle x-y \rangle_N + 1)$ and $\tilde{\mathbf{D}}_m(x,y) = \mathbf{D}_m(\langle x-y \rangle_N + 1)$, where $\tilde{\mathbf{A}}(x,y)$ denotes an entry standing in the x-th row and the y-th column of matrix $\tilde{\mathbf{A}}$; $\mathbf{A}(x)$ denotes the x-th components of vector $\mathbf{A}$, and $\langle n \rangle_N$ represents n modulo N. From the second equality of Eq. (3), the PN approximated by $\mathbf{J}_m$ could be estimated by the maximum likelihood estimation (MLE) or the linear minimum mean square error estimation (LMMSEE) [10], once $\mathbf{D}_m$ is known. Since LMMSEE requires much higher computational complexity, MLE is adopted throughout this work. Furthermore, $\tilde{\mathbf{H}}$ can be obtained by training symbols, and $\mathbf{S}_m$ can be estimated as $\mathbf{S}_m^{(0)}$ by making hard decision on $\tilde{\mathbf{H}}^{-1}\mathbf{R}_m$. When $\mathbf{D}_m^{(0)} = \tilde{\mathbf{H}}\mathbf{S}_m^{(0)}$ is obtained, $\mathbf{J}_m$ can be estimated as $\mathbf{J}_m^{(1)} = (\tilde{\mathbf{D}}_m^{(0)})^{-1}\mathbf{R}_m$.

Nevertheless, the knowledge of $\mathbf{J}_m^{(1)}$ does not help better estimation of $\mathbf{S}_m$ due to $\mathbf{S}_m^{(0)} = (\tilde{\mathbf{J}}_m^{(1)}\tilde{\mathbf{H}})^{-1}\mathbf{R}_m$. In order to reduce the error propagation from $\mathbf{S}_m^{(0)}$ to $\tilde{\mathbf{J}}_m^{(1)}$ and $(\tilde{\mathbf{J}}_m^{(1)}\tilde{\mathbf{H}})^{-1}\mathbf{R}_m$, the bandwidth of ICI must be truncated. Hence, $\mathbf{J}_m$ is modified as $\mathbf{J}'_m = [J_m(0), \cdots, J_m(L), 0, \cdots, 0, J_m(N-L), \cdots, J_m(N-1)]^T$, where $2L+1 \le N$. Notably, the definition of $\mathbf{J}'_m$ implies that $S_{m,q}$ and $S_{m,q'}$ will not mutually interfere, if $L < |q-q'| < N-L$. Hence, Eq. (3) can be written as,

#145131 - $15.00 USD Received 1 Apr 2011; revised 9 May 2011; accepted 9 May 2011; published 11 May 2011

$$\mathbf{R}_m \cong \tilde{\mathbf{J}}'_m \mathbf{D}_m + \mathbf{W}'_m = \tilde{\mathbf{d}}_m \mathbf{j}_m + \mathbf{W}'_m, \quad (4)$$

where $\tilde{\mathbf{J}}'_m$ is an $N \times N$ matrix with the entry of $\tilde{\mathbf{J}}'_m(x, y)$ equals to $\mathbf{J}'_m(\langle x - y \rangle_N + 1)$, and $\mathbf{W}'_m = (\tilde{\mathbf{J}}_m - \tilde{\mathbf{J}}'_m)\mathbf{D}_m + \mathbf{W}_m$ is the summation of the residual ICI and the white noise. Moreover, $\mathbf{j}_m = [J_m(0), \cdots, J_m(L), J_m(N-L), \cdots, J_m(N-1)]^T$ is a $(2L+1) \times 1$ vector, and $\tilde{\mathbf{d}}_m$ is an $N \times (2L+1)$ matrix obtained by removing the $(L+2)$-th ~ $(N-L)$-th columns of $\tilde{\mathbf{D}}_m$. As a result, after making hard decision to obtain $\mathbf{S}_m^{(0)}$ and $\tilde{\mathbf{d}}_m^{(0)}$, $\tilde{\mathbf{J}}_m'^{(1)}$ can be computed by calculating,

$$\mathbf{j}_m^{(1)} = (\tilde{\mathbf{d}}_m^{(0)H} \tilde{\mathbf{d}}_m^{(0)})^{-1} \tilde{\mathbf{d}}_m^{(0)H} \mathbf{R}_m, \quad (5)$$

where the superscript *H* denotes Hermitian transpose. Then, $\mathbf{S}_m^{(1)}$ obtained by making hard decision on

$$(J_m^{(1)}(0) \cdot \tilde{\mathbf{H}})^{-1} [\mathbf{R}_m - (\tilde{\mathbf{J}}_m'^{(1)} - J_m^{(1)}(0) \cdot \hat{\mathbf{I}}) \mathbf{D}_m] \quad (6)$$

is expected to show lower bit-error rate (BER) than $\mathbf{S}_m^{(0)}$ [10], where $\hat{\mathbf{I}}$ is an $N \times N$ identity matrix. Notably, $J_m^{(1)}(0) = \tilde{\mathbf{J}}_m'^{(1)}(1,1)$ in Eq. (6) represents the estimated PRT which is assumed common, and $(\tilde{\mathbf{J}}_m'^{(1)} - J_m^{(1)}(0) \cdot \hat{\mathbf{I}}) \mathbf{D}_m$ is the estimated ICI. Furthermore, $\mathbf{S}_m^{(i)}$ could replace $\mathbf{S}_m^{(i-1)}$ in the algorithm iteratively to get the better result of $\mathbf{S}_m^{(i+1)}$.

To summarize the algorithm, the simplified concept of the algorithm is depicted in Fig. 1 without considering the channel response, and it contains following three iterative steps:

i. making hard decision on the received signal to "guess" what the transmitted signal is

ii. estimating the PN from the received signal and the guessed transmitted signal by Eq. (5)

iii. removing the PN from the received signal by Eq. (6)

Since Eq. (5) requires a matrix inversion, it will dominate the computational complexity of the algorithm. Fortunately, the addition and multiplication needed by $(\tilde{\mathbf{d}}_m^{(0)H} \tilde{\mathbf{d}}_m^{(0)})^{-1}$ are $O(L^3)$, and *L* is generally small compared with *N* as a result of very limited computational complexity.

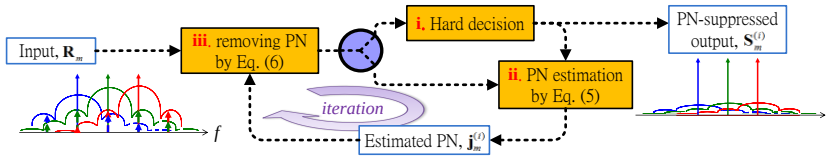

Fig. 1. Simplified PNS algorithm.

3. Experimental results and discussion

The experimental setup of an OFDM RoF system at 60-GHz band is shown in Fig. 2 [12]. The optical source is a DFB laser at 1555 nm, and its linewidth depends on the laser output power. In our experiment, the laser output powers of 10.5 dBm and 8.5 dBm are adopted, resulting in the measured linewidths of 1.3 MHz and 1.8 MHz, respectively. First dual-parallel modulator can produce an optical single-side band OFDM signal at 12 GHz, and second one up-converts the RF frequency to 60 GHz via frequency quadrupling [13]. The following 33/66 GHz interleaver with the 3-dB bandwidth of 32 GHz is used to filter out undesired optical signals. The real and imaginary parts of an electrical OFDM signal are generated by a Tektronix® AWG7102 arbitrary waveform generator (AWG). The sampling rate and D/A resolution of the AWG are 10 GHz and 8 bits, respectively, and the OFDM signal contains 176 subcarriers of 16-QAM format to occupy 7-GHz bandwidth with the fast-Fourier transform size of 256 and the CP of 1/16, yielding the data rate of 25.78 Gbps. After single mode fiber transmission, the electrical

#145131 - $15.00 USD Received 1 Apr 2011; revised 9 May 2011; accepted 9 May 2011; published 11 May 2011

7GHz-wide OFDM signal at 60 GHz is generated after square-law photo- detection in the 67-GHz photodiode. The generated OFDM signal is then amplified by a low noise amplifier (LNA) with 38-dB gain. After the LNA, the 60-GHz OFDM signal is fed into a rectangular waveguide-based standard gain horn antenna with ~23-dBi gain, and transmitted over 3-m wireless distance which is fixed and irrelevant to fiber length. After transmission over the air, the 60-GHz signal is received by another horn antenna and down-converted by a 55-GHz local

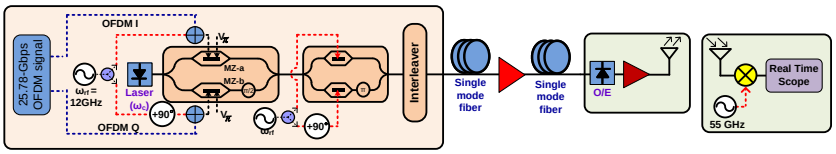

Fig. 2. Experimental setup of the 60-GHz RoF transmission system.

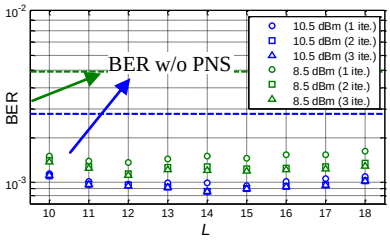

Fig. 3. The BER after iterative PNS algorithm as a function of *L*.

oscillator, an electrical 25.78-Gbps signal at 5 GHz is obtained and captured by a Tektronix® DPO 71254 with the 50-GS/s sampling rate and the 3-dB bandwidth of 12.5 GHz. The off-line DSP program is applied to demodulate the signal and carry out the PNS algorithm, and BER is measured by error counting.

Figure 3 shows the BER as a function of *L* with the received power of –6 dBm after 115-km fiber transmission and the proposed iterative PNS algorithm. The optimized *L* after three iterations is around 12~14, and further increasing *L* does not help the reduction of BER due to error propagation from $\mathbf{S}_m^{(i)}$ to $\mathbf{S}_m^{(i+1)}$. Notably, to achieve the best result, the values of *L* may vary with different iteration time, transmission distance and laser parameters, and it can be optimized by long training symbols in advance. Therefore, *L* is optimized for each time as the proposed algorithm is applied throughout our experiment, and it lies in between 10 and 16. Furthermore, Fig. 4 depicts the BER curves after 115-km fiber with and without the iterative PNS algorithm. Without any PNS, the signal cannot reach the FEC threshold (BER of 2×10^{-3}), but the BER is improved to lower than 2×10^{-3} with the proposed algorithm for both cases of 10.5-dBm and 8.5-dBm laser output power. Since the third iteration only provides little improvement as show in Fig. 4, three iterations approximately reach the best performance. Furthermore, the results employing ideal PNS with the perfect knowledge of $\mathbf{S}_m$ are also plotted for comparison, and the applied values of *L* are identical to those used in the first iteration. The further improvement by ideal PNS comes from the absence of error propagation, compared with the other iterative cases. However, the BERs employing ideal PNS are still worse than the case without dispersion-induced PN (B-to-B, with only air transmission), because of two assumptions made in the algorithm: 1) the bandwidth of ICI is limited to *L*, and 2) OFDM subcarriers are completely coherent after transmission. Therefore, the performance gap between the signals without PN and with PN suppressed by iterative PNS comes from both the incomplete knowledge of $\mathbf{S}_m$ and the assumptions of the algorithm.

Figure 5 plots the relative power penalty to reach the BER of 2×10^{-3} as a function of fiber distance before and after three time iterative PNS or ideal PNS. For both the cases of 10.5-dBm and 8.5-dBm laser output powers, their maximum transmission distances to reach the BER of

#145131 - $15.00 USD Received 1 Apr 2011; revised 9 May 2011; accepted 9 May 2011; published 11 May 2011

2×10^{-3} can be extended beyond 100 km by the proposed PNS scheme to meet the distance requirement of long-reach PONs. Using 3-dB power penalty as a criterion, ~50% transmission distance increment can be obtained via iterative PNS, as shown in Fig. 5. Moreover, when the fiber distance is shorter than 50 km, since the contribution of the dispersion-induced PN to total noise at the concerned BER of $\sim 2 \times 10^{-3}$ is relatively small, the improvement by iterative PNS

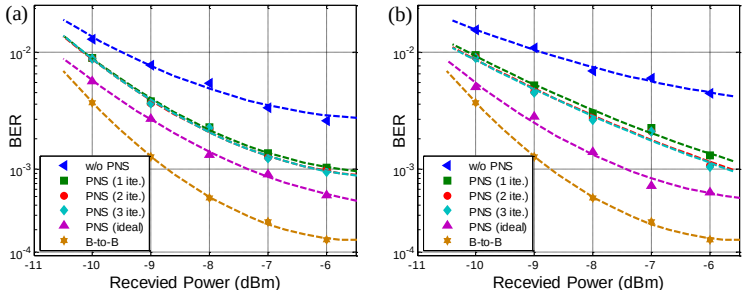

Fig. 4. BER curves after 115-km fiber with the laser power of (a) 10.5 dBm and (b) 8.5 dBm. (B-to-B: only 3-m air transmission).

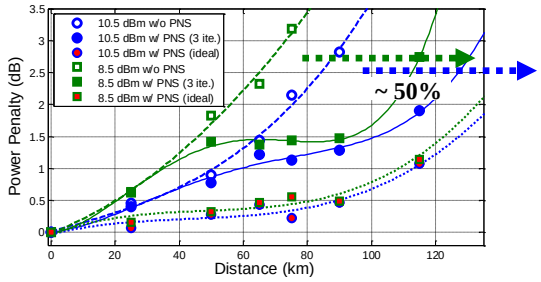

Fig. 5. Power penalty as a function of transmission distance.

is very limited. Consequently, as dispersion increasing, the benefit from iterative PNS increases, and the penalties are keep between 1 and 1.5 dB over the fiber distance of 50 km to 90 km. Nevertheless, even though errors at the concerned BER are mostly contributed by the dispersion-induced PN, the proposed scheme cannot always maintain the penalty under ~1.5 dB owing to unavoidable truncation of ICI bandwidth and the approximation of coherent subcarriers in the algorithm. This phenomenon can be understood by the increasing penalty of the signals with ideal PNS after 90 km, as shown in Fig. 5, since the issue of error propagation does not exist in the ideal PNS algorithm. Hence, the slopes of power penalties without and with PNS become similar after 90-km transmission.

4. Conclusions

In conclusion, a PNS algorithm is proposed to eliminate both PRT and ICI caused by the dispersion-induced PN in an OFDM RoF system at 60-GHz band. Thanks to the proposed algorithm, a commercial DFB laser with < 2-MHz linewidth could be applied to transmit 16-QAM OFDM RoF signals at 60-GHz band at the transmission distance of >100 km. For 25.78-Gbps 16-QAM OFDM signals generated by the laser with the linewidths of 1.3 MHz and 1.8 MHz, the proposed algorithm can extend the maximum fiber transmission distances corresponding to 3-dB power penalty from 75 km and 90 km to 115 km and ~135 km, resulting in ~50% improvement of transmission distance.

Acknowledgment

The authors would like to thank the NSC, Taiwan for financially supporting this research under Contract No. NSC-99–2221-E-009-047-MY3 and No. NSC 99-2218-E-260-003.

#145131 - $15.00 USD Received 1 Apr 2011; revised 9 May 2011; accepted 9 May 2011; published 11 May 2011